ADVANCED MATERIALS INTERFACES
Open Access
www.advmatinterfaces.de

Temperature Dependent Swelling Transitions of Hummers Graphite Oxide in Liquid 1-Alcohols

*Gui Li, Bartosz Gurzęda, Artem Iakunkov, Andreas Nordenström, Nicolas Boulanger, Christoph Hennig, Catherine Dejoie, and Alexander V. Talyzin**

Graphite oxides (GO) swell in liquid alcohols with significant expansion of c-lattice. However, temperature-dependent swelling of Hummers GO (HGO) has so far been reported only for methanol and ethanol. Here, HGO swelling in liquid 1-alchohols (C1 to C22 according to the number of carbons) is studied as a function of temperature using in situ synchrotron radiation XRD. Swelling transitions never previously observed for HGO in any kind of polar solvents are found, enthalpy of these transition and compositions of HGO-Cx solid solvates near the point of solvent melting reported. Swelling transitions from low temperature to high-temperature phase are found for HGO in C10–C22 alcohols, similarly to earlier reported transitions in Brodie graphite oxide (BGO). The transitions correspond to a strong change of inter-layer distance correlating with the alcohol molecules length and change in molecules orientation from perpendicular to parallel to GO planes (Type II transitions). However, Type I swelling transitions (related to insertion/removal of one layer of alcohol molecules) reported earlier for BGO are not found in HGO. Continuous changes of the d(001) spacing are revealed for HGO immersed in all smaller alcohols in the range C1 (methanol) to C9 (nonanol).

1. Introduction

Graphite oxides (GO) can be synthesized by strong oxidation of graphite using several methods. Fuming nitric acid is used to expand graphite lattice and a potassium chlorate is used to oxidize graphene sheets in the earliest Brodie method.[1] Hummers method is the most popular at the moment due to less dangerous and more rapid procedure which includes using concentrated sulphuric acid to expand graphite lattice and potassium permanganate as oxidant.[2] Several other methods have also been proposed for synthesis of GO, including, e.g., the Gurzeda method combining sulphuric acid with chlorates[3] or electrochemical method.[4] Despite the same "GO" name, these methods provide materials with rather different properties,[5] such as thermal exfoliation temperature range,[5,6] mechanical strength of individual flakes,[7] defect state[8] and swelling.[9] General for all of the oxidation methods is that mainly hydroxyl and epoxy groups are added to graphene planes, while the edges of graphene are functionalized mostly with carboxylic and carbonyl groups.[10] The inter-layer distance of GO increases up to 6–8 Å (compared to ≈3.3 Å in graphite) as a result of extensive functionalization with oxygen groups with the exact value depending on degree of oxidation and oxidation method.[10c]

Swelling in polar solvents is one of the properties of GO critical for several applications.[9a,11] Swelling occurs by sorption of solvents resulting in expansion of the inter-layer distance, typically characterized by X-ray diffraction (XRD) methods.[12] However, the solvent molecules intercalated in GO are completely disordered thus not allowing to determine orientation or packing of the molecules using XRD.[13] The liquid-like state of solvents intercalated into GO structure in combination with expanded c-lattices allows to use multilayered graphene oxide laminates produced from GO after dispersion and re-stacking of graphene oxide sheets as membranes.[14] The expansion of inter-layer distance by swelling is then a the critical parameter defining the size of "permeation channels" important in membrane applications.[14b–f] It is important to note that swelling of precursor GO and graphene oxide membranes can be rather different. For membranes it depends on air-ageing,[15] sample

G. Li, B. Gurzęda, A. Iakunkov, A. Nordenström, N. Boulanger, A. V. Talyzin
Department of Physics
Umeå University
Umeå SE-90187, Sweden
E-mail: alexandr.talyzin@umu.se
C. Hennig
Institute of Resource Ecology
Helmholtz-Zentrum Dresden-Rossendorf
Bautzner Landstrasse 400, 01328 Dresden, Germany
C. Hennig
The Rossendorf Beamline
European Synchrotron Radiation Facility
71 Avenue des Martyrs, Grenoble 38043, France
C. Dejoie
European Synchrotron Radiation Facility, ID22 Beamline
71 Avenue des Martyrs, Grenoble 38043, France

The ORCID identification number(s) for the author(s) of this article can be found under https://doi.org/10.1002/admi.202400651

DOI: 10.1002/admi.202400651

thickness,[16] oxidation degree,[17] flake size, and possibly several other parameters.[18] Therefore, studies of swelling performed using GO's are of the most fundamental value.

Swelling of GO in several polar solvents has been studied in recent decades as a function of temperature and pressure.[11b] Following the discovery of pressure-induced swelling,[19] swelling transitions related to change in amount of intercalated solvent were found also in the temperature-dependent experiments.[9d,20] The swelling transitions occur with sharp changes of GO interlayer distance due to insertion of solvent layer from liquid phase during the cooling and removal of this layer from GO structure upon heating half of temperature cycle.[9d,21] In fact, swelling transitions in liquid-immersed Brodie graphite oxide (BGO) provide possibly the best method to determine experimentally the thickness of single solvent layers.

Swelling of GO in 1-alcohols is the best studied at the moment, but mostly for small alcohols, such as ethanol and methanol.[12,15a,19b,21e,22] Swelling of BGO in liquid 1-alcohols with molecular chains longer than octanol was extensively characterized in our recent studies extending detailed structural characterization of BGO-alcohol systems up to C22 (behenyl alcohol).[23] In the following 1-alcohols will be named shortly by the number of carbon atoms in the chain (e.g., C8 for octanol). These studies revealed existence of two sharply different types of swelling transitions for BGO immersed in shorter alcohols (C1–C9) and long alcohols (C > 10). The 1-alcohol molecules in the set C1–C9 are intercalated into BGO forming structures with the solvent molecule layers oriented parallel to GO planes. This is verified by several methods, including TGA.[22b,c] Cooling the solvates in excess of solvent has been found to result in swelling transitions corresponding to the insertion of additional 1-alcohol layer for BGO upon cooling in liquid methanol, ethanol,[9d] propanol,[21e] heptanol,[22b] octanol,[22c] and nonanol.[22c] The Type I phase transitions are related to changes in the number of intercalated solvent layers (typically by only one) parallel to the graphene oxide plane orientation. The Type I phase transitions were not found in BGO systems with few other alcohols, such as pentanol and hexanol.[11b,22b] Intercalation of 1-alcohols longer than nonanol (C9) into GO (synthesized by the Staudenmayer method[24]) was reported in the 1960s and later confirmed in the 1980s for Brodie GO (BGO) but only as a part of PhD thesis published in German.[25] Enormously large lattice expansion is found for BGO swelling in longer 1-alcohols with inter-layer distances up to ≈50Å for C18.[26] Our recent temperature-dependent studies of BGO swelling in excess of long alcohols (C > 10) revealed reversible phase transitions with a decrease of interlayer distance and change in the orientation of the intercalated molecules from perpendicular to the GO planes in the ambient temperature α-phase to parallel in the high-temperature β-phase.[23a] This kind of swelling transition was named Type II as it is distinctly different from Type I transitions found for BGO immersed in shorter alcohols. Both Type I and Type II transitions observed in BGO heated in an excess of liquid alcohols should be considered as incongruent melting.[21b] Part of the solvent intercalated in BGO interlayers at low temperature is released into the liquid phase above the point of incongruent melting. Therefore, very general trends in swelling of BGO in the whole set of 1-alcohols (C1–C22) are known by now with data available for changes in interlayer distance, composition of low-temperature solvate phases, and enthalpy of transitions between low temperature and high-temperature phases.[23a]

In contrast, swelling of most commonly used in all applications Hummers graphite oxide (HGO) has so far been surprisingly little studied. It is known that more defect state of HGO[7,9b,15] results in less ordered structures of solvate phases at ambient temperature and absence of swelling transitions.[21c] Temperature-dependent swelling of HGO has been so far studied only in two alcohols, ethanol, and methanol, revealing gradual shift of (001)-reflection over interval of temperatures where these alcohols appear in liquid state.[9d] It should be noted that the changes of d(001) values are smaller than the size of solvent molecules. This is commonly explained by random interstratification[27] and more exotic intrastratification.[28]

In this study, we report synchrotron radiation XRD study of temperature-dependent swelling of HGO for the whole set of 1-alcohols starting from methanol (C1) to 1-docosanol (C22). Analysis of 20 HGO-alcohols systems includes also evaluation of solvent sorption near the point of melting using DSC method. Swelling transitions of Type I, very common in BGO-alcohol systems, were not found for HGO. However, Type II swelling transitions were revealed for HGO in the same range of alcohols as in BGO (C > 10). Therefore, our study provides the first report of swelling transitions in HGO. Enormous lattice expansion is found for swollen HGO with d(001) values up to 63.4 Å in liquid C22 near the temperature of its melting point. Since the melting point of these alcohols is above the ambient temperature, solid solvate phases are formed by HGO intercalated by long alcohols after solidification of molten solvent during the cooling. The swelling of BGO and HGO is compared for all systems with alcohols in the range C1–C22 providing the so far most comprehensive fundamental knowledge about GO swelling in 1-alcohols.

2. Results and Discussion

Swelling of HGO in a set of normal 1-alcohols (C1–C22, except C21 and C19) was studied here as a function of temperature using XRD and DSC. Detailed characterization of the HGO precursor is provided in Supporting Information file (Figures S1,S2 and S3, Supporting Information).

The study is mostly focused on the temperature region where the alcohols are in liquid state and limited to temperatures below 373 K to ensure absence of thermal degradation of HGO which occurs already ≈400–420 K.[9b,13] Alcohols C1–C11 are liquids at ambient temperature. Therefore, swelling of HGO in these alcohols was first tested in liquid-immersed state at ambient temperature, then the samples were cooled below the freezing point of solvent and heated back to ambient temperature or slightly above to verify if some changes were detectable. For larger alcohols, solid materials (HGO and alcohol) were mixed in a proportion that ensures saturated swelling of HGO after alcohol melting. The samples were heated over the melting point of alcohol and up to 373 K and finally cooled down back to ambient temperature.

It is known from earlier studies, that swelling affects only interlayer distance of GO structure thus producing shifts in position of (00ℓ)-reflections leaving other reflections corresponding to in-plane lattices unchanged. Therefore, complete information about temperature-dependent swelling of HGO in alcohols is provided by following evolution of the (00ℓ) set of reflections, which

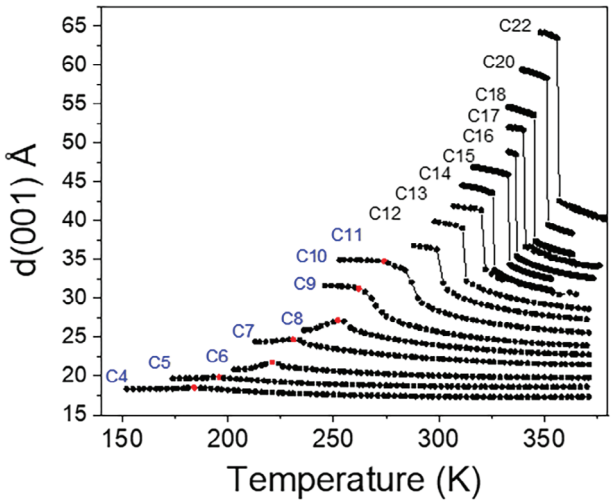

Figure 1. Temperature dependence of d(001) recorded from HGO-Cx samples during heating. Cx is the number of carbon atoms in 1-alcohol (C4–C22). Alcohols that are liquid at ambient temperature are shown by blue symbols, red points correspond to the start of alcohol melting detected by XRD. For several longer alcohols, the data recording started just above the melting of alcohols.

corresponds directly to the averaged distance between the graphene oxide planes in a swollen structure. The number of reflections observed for this set is rather different for HGO swollen in shorter (1-2 reflections) and longer alcohols (up to 15). Therefore, we decided to use the d(001) value for comparing the data for HGO in all alcohols. Temperature dependence of d(001) recorded during the heating part of the temperature cycle is shown in **Figure 1** for alcohols C4–C22. HGO swelling in these alcohols shows almost no hysteresis in d(001) value recorded during cooling and heating. The swelling of HGO in smaller alcohols will be discussed separately below.

Analysis of data shown in Figure 1 can be summarized as follows:

1) The expansion of HGO c-lattice due to swelling is proportional to the length of 1-alcohol molecules. **Table 1** shows the values of d(001) recorded from HGO-Cx samples just above the melting point of alcohol (α-phases). The highest value of d(001) = 64.2 Å is found for HGO-C22. In average the increment of d(001) is ≈2 Å per carbon atom added to the molecular chain.
2) Two rather distinct types of d(001) temperature dependence are obvious in Figure 1. Sharp phase transitions are found for long alcohols HGO-Cx with X = 10–22 (Type A). An almost flat temperature dependence of d(001) above the melting point of alcohols is found for HGO in shorter alcohols (C4–C8). Some gradual changes of d(001) are observed even for these alcohols and become somewhat stronger for C7 and C8 (Type B).
3) HGO in C9 is an "intermediate" case as it still shows gradual changes of inter-layer distance resembling temperature dependence in smaller alcohols, but also a significant change resembling phase transitions observed for longer alcohols.

Below we provide more detailed analysis of XRD data for the systems with Type A and Type B temperature dependence of HGO swelling. XRD data for HGO systems with other 1-alcohols are provided in Supporting Information file. Table 1 shows summary of the most important quantitative characteristics of HGO swelling in all 1-alcohols studied here. It is also important to note that HGO phases formed in 1-alcohols with melting temperature above the ambient are preserved after solvent solidification thus providing solid solvates stable at ambient temperature. The alcohol molecules are weakly bound (most likely by hydrogen bonding) to the GO sheets as evidenced by possibility to dissolve all intercalated alcohol by washing with ethanol thus recovering precursor HGO (see example for HGO-C16 system in Supporting Information file).

Figure 2a shows the XRD patterns recorded from the HGO-C20 sample starting from the temperature just above the melting point of alcohol. Below the temperature of alcohol melting, the sample is simple mixture of HGO and solid C20. Melting of C20 results in immediate formation of HGO-C20 solvate phase with d(001) = 59.1 Å. This value is ≈52 Å larger compared to the inter-layer distance of precursor HGO. Further heating results in a swelling transition obvious from the step-like decrease of the interlayer distance ≈351 K. It should be noted that swelling transitions have so far never been reported for HGO in any solvents.

This transition has all the characteristic features earlier reported for Type II phase transitions in BGO-long alcohol systems.[23c] Our results show that the same type of phase transition is found also for HGO in all long alcohols (C > 9). An example of HGO-C20 (Figure 2) shows all typical features also found

Table 1. Summary of structural information for solid HGO-alcohol solvate phases (from left to right): melting point of pure alcohol, d(001) value recorded just above the temperature of alcohol melting after intercalation of alcohol into HGO structure, composition of HGO-Cx just above the melting point of alcohol calculated using DSC method.

System	Melting point [K]	$d(001)_{\text{After melting}}$ [Å]	Composition [g/g]
HGO-C1	175	19.6	1.12
HGO-C2	159	23.2	/
HGO-C3	147	22.7	/
HGO-C4	183	18.5	1.21
HGO-C5	195	19.9	1.01
HGO-C6	228	21.1	1.05
HGO-C7	238	24.0	0.97
HGO-C8	257	26.2	1.28
HGO-C9	267	30.0	1.25
HGO-C10	279	34.1	1.61
HGO-C11	292	36.5	1.97
HGO-C12	297	39.8	2.00
HGO-C13	305	41.8	2.09
HGO-C14	311	44.5	2.14
HGO-C15	315	46.8	2.21
HGO-C16	322	48.8	2.26
HGO-C17	327	51.9	2.70
HGO-C18	332	54.1	2.61
HGO-C20	337	59.1	2.98
HGO-C22	343	63.6	3.16

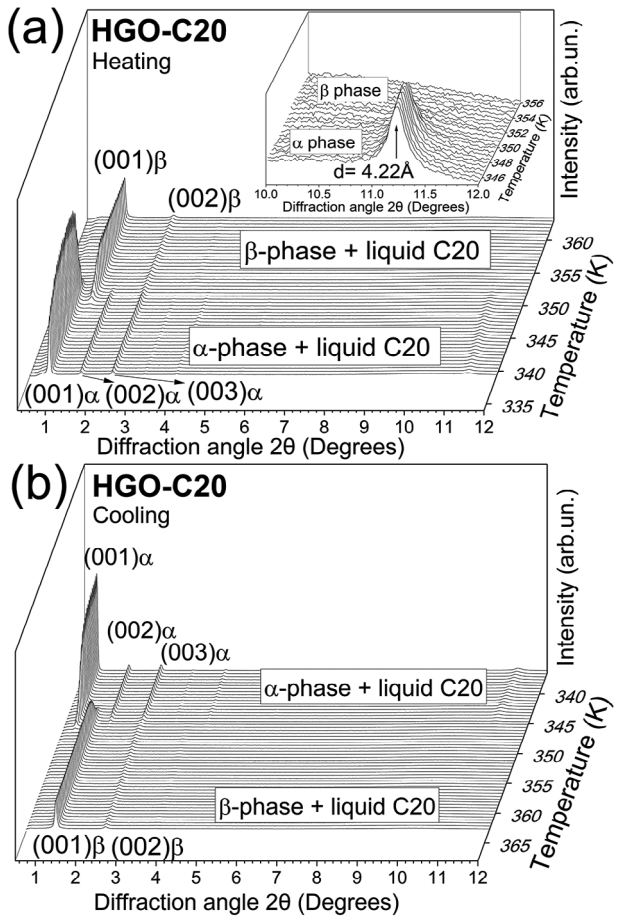

Figure 2. XRD patterns recorded from the HGO-C20 sample premixed as powders with excess of alcohol required for saturated swelling and heated over the temperature of C20 melting. The figure is limited to temperature interval above the melting point of C20 with selected patterns recorded during heating (a) and cooling (b), ($\lambda = 0.7381$ Å).

for HGO immersed in other alcohols (C10–C22) and for BGO swelling transitions in the same alcohols.

The structure of the low temperature α- phase consists of two layers of alcohol molecules with orientation perpendicular to the graphene oxide planes. The increment of d(001) by ≈52 Å corresponds approximately to the double length of C20 alcohol molecule. The packing of C20 molecules is "solid-like" exhibiting one additional reflection with d-spacing of 4.22 Å. As discussed in our earlier studies, this d-spacing corresponds approximately to the diameter of long-chain alcohol molecule considered as a cylinder.[23b,c] The absence of other reflections from intercalated alcohol molecules allows to suggest that the structure of vertical double layer of C20of is formed by closely packed molecular "cylinders" nearly completely disordered relative to each other. Exact composition of α-phases was determined using the DSC method (**Table 2**). The method is based on measurements of enthalpy of alcohol melting. The amount of liquid alcohol in a molten phase decreases due to sorption and intercalation of the solvent into the HGO structure. Therefore, the melting enthalpy of alcohol measured from HGO-C_x sample is smaller compared to reference enthalpy of pure alcohol. Knowing the exact amount of alcohol loaded into a sample and the enthalpy of alcohol melting, it is possible to calculate the amount of alcohol sorbed (intercalated) into HGO structure. This method was extensively used in earlier publications for evaluation of liquid solvent sorption by GO materials.[21b,22b]

The Type II swelling transition corresponds to the incongruent melting of the α-phase with part of alcohol escaping the structure into a liquid phase and the remaining part forming layers parallel to graphene oxide planes.[23b,c] The interlayer distance of β-phase formed above the point of transition is significantly smaller (d(001) = 39.5 Å for HGO-C20). It should be noted that composition of the β-phases is difficult to evaluate due to low vapor pressure of alcohols in the given temperature interval limited by ≈380 K due to thermal degradation of GO. Therefore, it is impossible to use simple vapor sorption method to evaluate composition of GO materials after saturated sorption is achieved at a given temperature.[18b,22a–c] Approximate composition of the β-phase was reported previously only for the BGO-C16 system after extensive and rather time-consuming experiments with samples of BGO and C16 components mixed in different proportions.[23b]

The swelling transitions of Type II are reversible as demonstrated by the XRD data collected during the cooling (Figure 2b for HGO-C20, for other systems, see Supporting Information file).

The reversible Type II transitions are also easily detected by DSC due to appearance of new peaks in addition to the anomalies related to alcohol melting and solidification (**Figure 3**). The HGO was mixed in these experiments with powder of alcohols in a proportion providing excess of alcohol after saturated sorption by HGO. The samples were initially heated above the melting point of alcohol to form HGO-Cx by saturated sorption and cooled back to ambient temperature. The DCS scans shown in Figure 3 were recorded in the next heating-cooling cycles performed with samples including (at ambient temperature) pure alcohol and solid phase of HGO-Cx. The DSC scans recorded from HGO-C9 show only anomalies related to melting and solidification of excess alcohol not sorbed by HGO (Figure 3b) at the same temperatures as in the reference DSC scan of pure alcohol (Figure 3a). No anomalies due to swelling transitions were found in HGO-C9 and HGO with other shorter alcohols. DSC scans recorded from HGO-Cx samples with x = 10 and longer demonstrate additional features related to reversible incongruent melting (swelling transitions) (Figure 3d,f, see also Figures S30–S38, Supporting Information for HGO with other alcohols).

The DSC scans recorded from pure C20 (Figure 3d) (and several other long alcohols) also show additional features related to solid-solid transitions. Note that mixing HGO with Cx in a proportion not sufficient for saturated sorption is likely to result in formation of additional phases and additional anomalies, as it was earlier found in detailed study of BGO-C16 system.[23b] However, in this study we focused only on HGO-Cx phases formed after saturated sorption of alcohols.

Enthalpies and temperature points of swelling transitions found for HGO in longer alcohols are summarized in Table 2. The enthalpy of Type II swelling transition increases with the length of alcohols with maximal value of 0.46 kJ g^{-1} found for HGO-C22. This trend reflects stronger interaction between longer alcohol molecules packed approximately parallel to each other. The temperature points of swelling transitions are also

Table 2. Summary data related to swelling transitions found for HGO in a set of 1-alcohols C10–C22. From left to right: temperature of pure alcohol melting, enthalpy of swelling transition according to DSC data (per gram of HGO), d(001) value for α-phase just before transition, d(001) value for β-phase just after transition.

System	Onset T [K]	Enthalpy [kJ/g, HGO]	$d(001)_{\text{Before transition}}$ [Å]	$d(001)_{\text{After transition}}$ [Å]
HGO-C10	277	0.07	33.6	29.4
HGO-C11	287	0.10	36.2	31.1
HGO-C12	308	0.15	39.0	32.2
HGO-C13	320	0.18	41.3	33.2
HGO-C14	327	0.25	43.5	33.6
HGO-C15	333	0.27	45.9	34.3
HGO-C16	338	0.27	48.5	35.5
HGO-C17	342	0.36	51.6	36.6
HGO-C18	346	0.35	53.6	37.4
HGO-C20	352	0.40	58.3	39.5
HGO-C22	357	0.46	63.4	42.5

correlated with the length of alcohol and higher melting points of pure alcohols. Some other general trends related to Type II phase transitions in HGO and BGO systems are considered below in the discussion section.

The similarity between temperature dependences of BGO and HGO swelling is rather surprising considering very strong difference observed for swelling in smaller alcohols (C < 10). The example of Type B temperature dependence is shown in **Figure 4** for d(001) of HGO immersed in liquid pentanol (C5).

XRD patterns of HGO recorded in liquid pentanol showed (001) and (002) reflections with positions almost unchanged during cooling down to the point of pentanol solidification. The d(001) value recorded at 301 K is 18.65 Å. Cooling results in gradual and continuous increase of d(001) up to 19.9 Å at 193 K. The change by ≈1.2 Å is clearly smaller than the thickness of one pentanol layer even if it was oriented parallel to the GO planes.

The continuous changes in d(001) values are commonly explained for layered hydrophilic materials by the effects of random interstratification[28b] or by intrastratification.[28a] In both cases, it is assumed that GO interlayers include discrete number of intercalated solvent layers (e.g., 1,2,3, etc) but due to random packing of these layers only one (001) reflection is observed with the position of this reflection shifting as function of changes in the relative number of differently solvated inter-layers. Interstratification is common in swollen GO,[28b,29] clay minerals[30] and MXenes.[31] The value of d(001) should not be directly equalized with "inter-layer distance" of HGO-C5 structure since the changes are much smaller than the size of the molecule inserted into the structure. The d-spacing for c-lattices needs to be considered as averaged value with real inter-layer distance still corresponding to the size of intercalated molecules. Considering the thickness of one pentanol layer parallel to HGO planes to be ≈4 Å and ≈11.6 Å lattice expansion due to swelling, the room temperature phase is likely to be intercalated with three layers of pentanol while the increase of d(001) at low temperature indicates that some interlayers start to be intercalated with 4 layers of solvent. Taking the HGO-C8 system as another example, the difference between d(001) values observed at 370 K (22.77 Å) and at 255 K (27.0 Å) is ≈4.2 Å. This value corresponds roughly to the insertion of one additional octanol layer but occurs over broad temperature interval unlike BGO where sharp step-like swelling transition with similar change of d(001) was earlier found.[22c] BGO immersed in liquid octanol at room temperature forms solvated structure with four layers of solvent parallel to GO planes. Cooling BGO in excess of octanol results in a swelling transition into five-layer structure considering the thickness of one layer to be 4.5 Å.[22c] The phase transformations in HGO-pentanol system can be explained assuming strongly inhomogeneous oxidation of this type of GO as compared to more homogeneously oxidized BGO. The temperature dependence observed for HGO in, e.g., octanol can be interpreted in a way that each interlayer of differently oxidized regions on graphene oxide planes has its own slightly different temperature of swelling transition from four-layer to five-layer phase. As a result, the sharp transition observed in BGO-C8 system is smeared over much broader interval of temperatures due to averaging over many parts of the sample where transition occurs at somewhat different temperature point.

So far, discussion of the temperature-dependent swelling of HGO in alcohols did not include smallest alcohols: methanol, ethanol, and propanol (C1–C3). That is, because HGO in these alcohols is not following exactly the trends shown in Figure 1. The temperature-dependent swelling of HGO in these solvents shows no sharp transitions and can be described as Type B but with significantly stronger changes of d(001) between ambient temperature and the temperature point of solvent solidification. Methanol and ethanol are the only alcohols for which HGO swelling was studied earlier reporting "enormous" lattice expansion at low temperatures.[21c] We re-recorded the temperature dependences for these solvents with new data providing much better signal-to-noise ratio and time resolution (see **Figure 5** for HGO in methanol and Figures S4–S6, Supporting Information for ethanol and propanol)). The d(001) = 13.26 Å value recorded from HGO immersed in methanol at 312 K gradually increases upon cooling until the point of alcohol solidification reaches the value 19.67 Å. The increment by ≈6.4 Å corresponds approximately to the thickness of two methanol layers. The thickness of one methanol layer is known exactly from experiments with BGO-methanol system. The swelling transition reported earlier for BGO immersed in methanol is related to change from one-layer structure at ambient temperature into two-layer structure

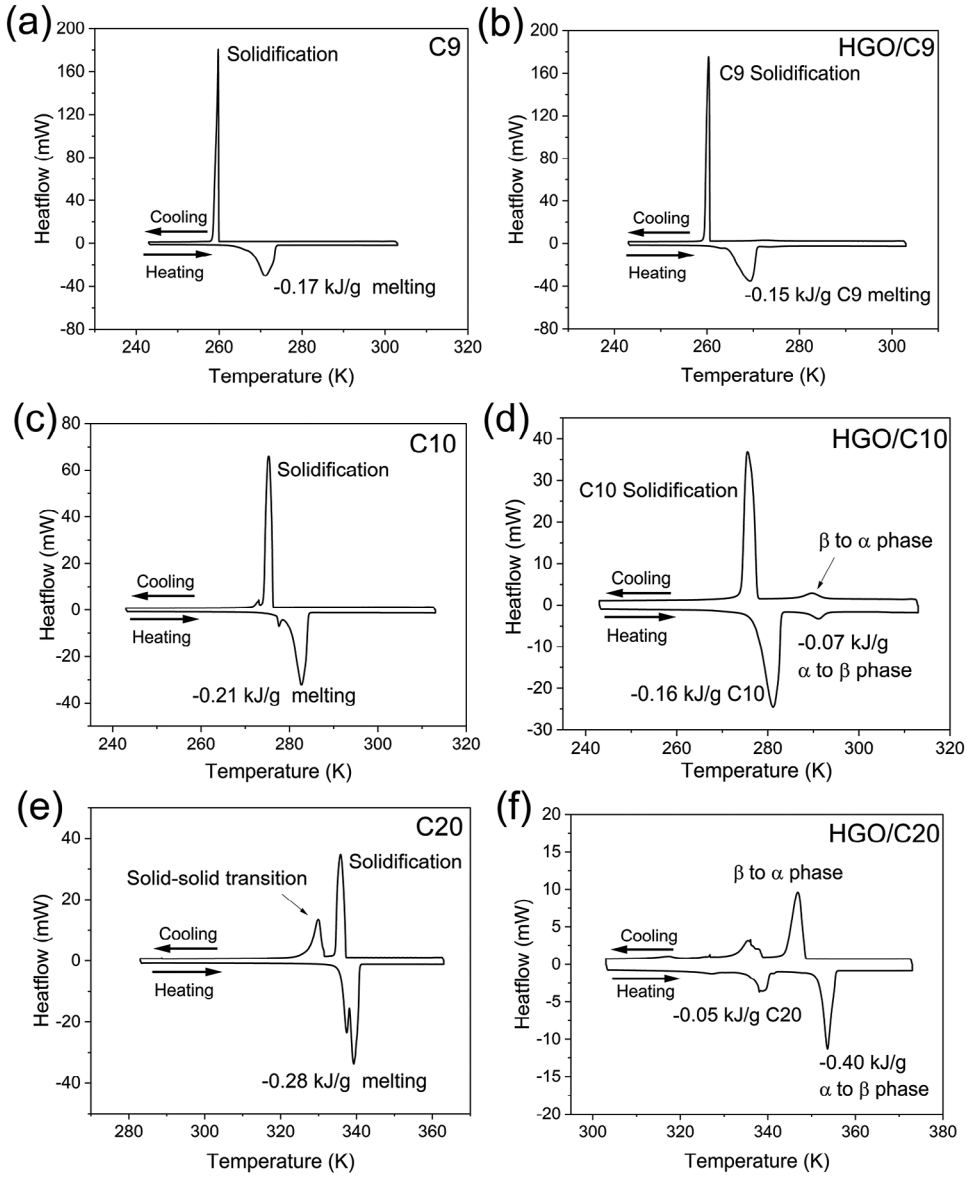

Figure 3. DSC scans recorded from pure 1-alcohols and the same alcohols with added HGO powder. Scan recorded from pure C9 (a) and HGO/C9 (b) show only anomalies from melting and solidification of alcohol. Pure C10 (c) and C20 (e) show anomalies related to melting and solidification of alcohol and anomalies due to solid-solid transitions. Scans from HGO/C10 (d) and HGO/C20 (f) demonstrate additional anomalies due to reversible Type II (α to β phase) swelling transitions.

at low temperatures with step-like change of the d(001) value by 3.3 Å.

The structure of HGO in liquid methanol is expanded significantly stronger compared to the BGO-methanol system. Considering ≈7 Å c-lattice parameter in the solvent-free HGO and ≈3.3 Å thickness of methanol layer, the d(001) = 13.26 Å corresponds to the insertion of two methanol layers parallel to GO planes already at ambient temperature. Considering again the effects of interstratification and gradual changes of d(001) observed upon cooling, some interlayers of HGO get intercalated first with three layers of methanol and at lowest temperature with four layers of methanol (Figure 5a). A sudden drop in the d(001) value corresponding approximately to the size of two methanol layers is observed below the point of methanol melting. This drop is likely related to partial escape of methanol from the GO structure, similar to the previously observed anomalies in BGO and HGO swollen in water.[32] No similarly strong change is found below the freezing point of ethanol in the HGO-C2 system (Figure 5d). The difference between composition of methanol solvates close to the melting point of methanol is also obvious from the analysis of DSC data. The sorption of methanol by HGO measured by DSC in this study was 1.12 g/g (in agreement with earlier studies reported in ref. [21b]) compared to 0.55 g/g reported for BGO.[22a] For HGO immersed in ethanol the difference between d(001) values measured at 352 K (15.0 Å) and 170 K (23.41 Å) is ≈8.4 Å (Figure 5d). Considering the thickness of an ethanol layer

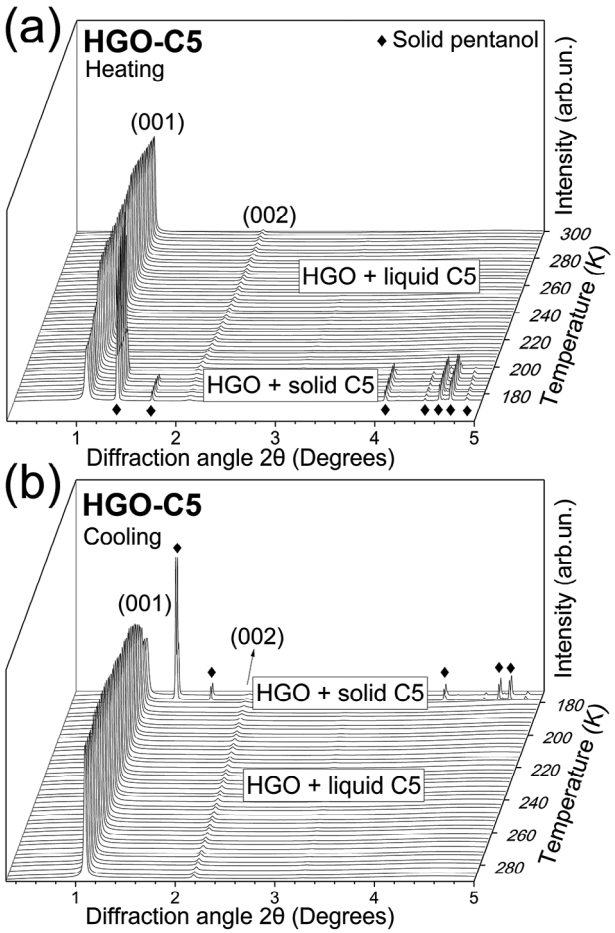

Figure 4. XRD patterns recorded from HGO sample immersed in excess of liquid pentanol (C5) during heating (a) and cooling (b). Relections from solid pentanol are marked by ♦ symbols, (λ = 0.354352 Å).

≈4 Å (ref. [9d]) this change corresponds to the insertion of two additional layers and an overall composition at the lowest temperature corresponding to four ethanol layers. Finally, for HGO in propanol the difference between low and high-temperature solvates is ≈5.3 Å with maximal value of d(001) = 22.67 Å (Figure S6, Supporting Information). The maximal sorption of propanol by HGO is also then close to expected value for four-layer phase. Considering rather strong change in d(001) value between ambient and low-temperature HGO solvates it is convenient to group swelling in methanol, ethanol, and propanol into Type C to distinguish it from Type B (C4–C9) and Type A (C10–C22) in the following discussions.

Some specific features found for HGO swelling in group C1–C3 could possibly be related to water impurities since methanol, ethanol, and propanol are solvents that are completely miscible with water and easily absorb water from air. Note however that swelling of BGO was previously studied for methanol-water mixtures revealing shift in the temperature point of swelling transitions but not in the value of d(001) change.[22a]

It is interesting to discuss in more detail some general trends observed for swelling of HGO in the whole set of alcohols studied here (C1–C22) and to compare swelling of HGO with earlier reported swelling of BGO in the same set of 1-alcohols. Sorption of 1-alcohols by HGO and BGO is compared in **Figure 6**a. The sorption corresponds to composition of GO-Cx found at low temperatures close to the point of relevant Cx alcohol melting.

Figure 6 shows two very distinct regions for HGO sorption. Compositions of all HGO solvates with alcohols in the range C1–C9 are approximately the same (1.1–1.2 g/g) whereas for alcohols C10–C22 the sorption increases proportionally to the length of the molecules. These two regions correspond to different solvate structures. Our data suggests that 1-alcohols C1–C9 are intercalated into HGO as layers parallel to GO planes. Considering XRD data, it is likely that about four layers of alcohol molecules are intercalated close to the melting point of solvent. The "weight" of one solvent layer with orientation parallel to GO planes is obviously similar for nearly all close-packed alcohol molecules (≈0.3 g/g). When alcohol molecules are forming layers in a "stand up" orientation approximately perpendicular to GO planes, the thickness of one layer is proportional to the length of molecules. Therefore, the sorption of alcohols C10–C22 in g/g units increases approximately linearly in accordance with XRD data showing that the inter-layer distance proportionally increases with the length of molecules (Figures 1 and 7 and Table 1).

A linear trend is also observed for both BGO and HGO swelling transitions in alcohols C10–C22. Once again, HGO shows no sharp swelling transitions in alcohols C1–C9. The change in interlayer distance at the point of transition is plotted versus the length of alcohol in **Figure 7**. Remarkably the HGO and BGO show nearly identical slopes in this figure, but HGO transitions are smaller by ≈4 Å which corresponds roughly to the thickness of one alcohol layer (parallel to GO planes). Moreover, the enthalpy of transitions is somewhat smaller in average for HGO as compared to BGO (Figure 6b).

The orientation of alcohol molecules changes from perpendicular (α-phase) to parallel (β-phase) to GO planes. Our earlier study suggests that the number of parallel layers in the β-phase increases for longer alcohols. The data shown in Figure 7 suggests that β-phases of HGO are either intercalated by less alcohol or orientation of alcohol chains in HGO is not strictly perpendicular to GO planes in the α-phases. The solvent is intercalated into GO structure of β-phases in a "liquid-like" and completely disordered state. Smaller inter-layer distance of the HGO β-phases cannot be related to different oxidation degree since the BGO studied in ref. [23a] has somewhat larger C/O ratio).

It is more likely that somewhat smaller sorption of long alcohols by HGO and smaller change in inter-layer distance due to swelling transitions is related to more inhomogeneous distribution of oxygen groups in HGO and existence of isolated nm-sized non-oxidized regions,[33] in contrast to more homogeneously oxidized and less defect BGO. The less perpendicular orientation of alcohol molecules can be related to non-oxidized regions on GO planes where alcohol molecules cannot attach to graphene sheets due to the lack of oxygen groups. Therefore, some "empty" space over the non-oxidized regions is available. This space can possibly be filled if orientation of alcohol molecules is less perpendicular, luting toward the space over non-oxidized regions. However, our data does not allow unambiguous interpretation for difference in the magnitude of inter-layer distance change between BGO and HGO systems with long alcohols.

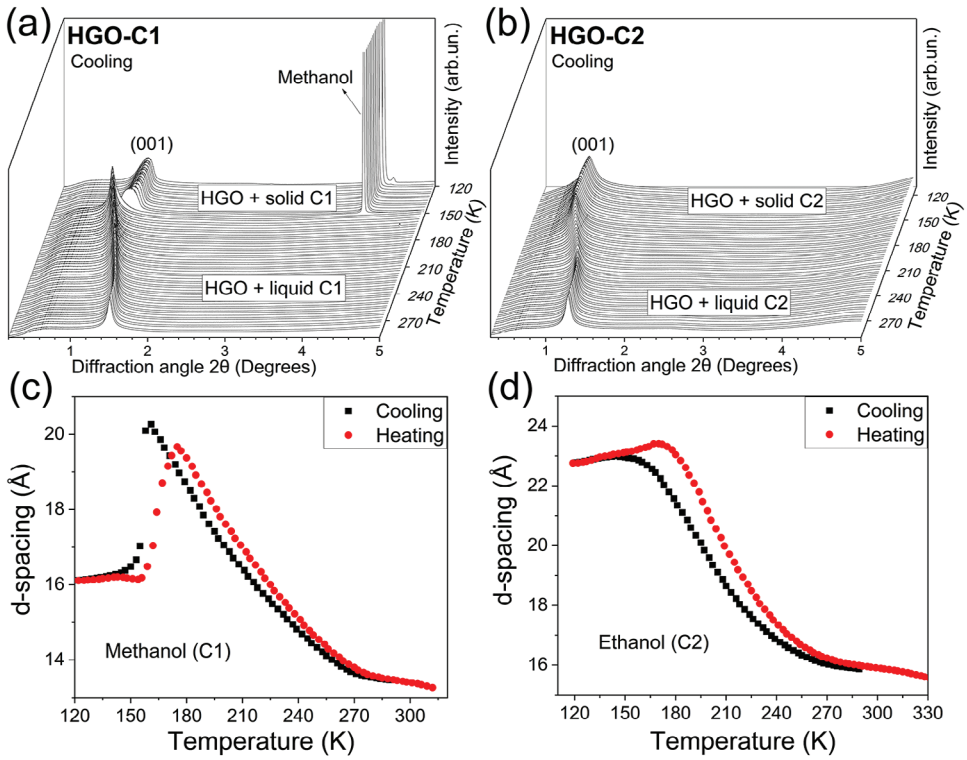

Figure 5. Diffraction patterns recorded from HGO immersed in alcohols as a function of temperature during cooling to temperatures below the point of solidification: a) HGO in methanol, b) HGO in ethanol. c) Temperature dependence of d(001) for HGO recorded in liquid methanol and d) liquid ethanol ($\lambda = 0.35435$ Å).

Finally, some very general considerations can be suggested to explain similarities between swelling of HGO and BGO in longer alcohols and dissimilarities for swelling in short alcohols. Considering thickness of one GO layer of ≈7 Å, ≈90% of the total unit cell volume in the low-temperature HGO-C22 structure (c = 63.6 Å) is occupied by two vertical layers of alcohol molecules. Even for the structures formed by swelling of BGO and HGO in C10 the proportion of cell volume occupied by GO layers is only ≈20%. Therefore, it is not surprising that the properties of both BGO and HGO phases are mostly defined by the structural arrangement of long alcohol molecules forming 2D (but poorly ordered) crystal structure confined between graphene oxide sheets.

We suggest that rather similar swelling transitions observed in both BGO and HGO systems with alcohols C10–C22 are mostly related to the properties of 2D alcohol crystals rather than to properties of graphene oxides. The swelling transitions from α- to β-phase should be described strictly speaking as incongruent melting of α-phase. Therefore, it is not surprising that higher temperature points of swelling transitions observed for both BGO and HGO systems with longer alcohols (Table 2) correlate with higher melting points of pure alcohols (Table 1).[23a] Moreover, the structure of low-temperature α-phases of GO with long alcohols can be described as "solid" while high-temperature β-phases have been cited previously as "liquid-like" with reference to the state of alcohol molecules confined between graphene oxide sheets, thus extending analogy with melting of pure alcohols.[22d]

Long alcohols are essentially hydrophobic due to the long hydrophobic hydrocarbon chain and hydrophilic only at the end terminated by —OH group. Therefore, the longer is alcohol molecule, the more important (for overall properties of the material) will be van der Waals interaction between the hydrophobic alcohol chains in the 2D crystal structure. At the same time the overall importance of hydrogen bonding between hydrophilic —OH groups and oxygen groups on graphene oxide sheets remain the same independently on the length if the molecules are oriented perpendicularly to the GO planes.

As suggested in our previous study of BGO swelling, the change of alcohol molecule orientation from parallel to perpendicular (relative to graphene oxide) for structures with longer alcohols (C > 10) is likely related to repulsion of long hydrophobic hydrocarbon chains from hydrophilic graphene oxide surface.[23b] Gradual increase of the alcohol chain also generates additional effects related to possible formation of kink-layers.[23a] Longer molecules oriented parallel to graphene oxide sheets in random in-plane orientations will overlap over each other forming multilayer structures in completely disordered β-phases of both BGO and HGO. The number of possible "kink-layers" is proportional to the length of the molecules.[23a] It is likely that kink-layered structures can be formed by alcohols longer than C10 considering ≈4 Å diameter of alcohol molecules and simple geometric considerations.[23a]

The properties of BGO and HGO phases formed by swelling in shorter alcohols are defined to a much larger extent by the properties of graphene oxide sheets and interactions between oxygen functionalities of graphene oxide with -OH groups of alcohol molecules. The absence of well-defined swelling transitions in

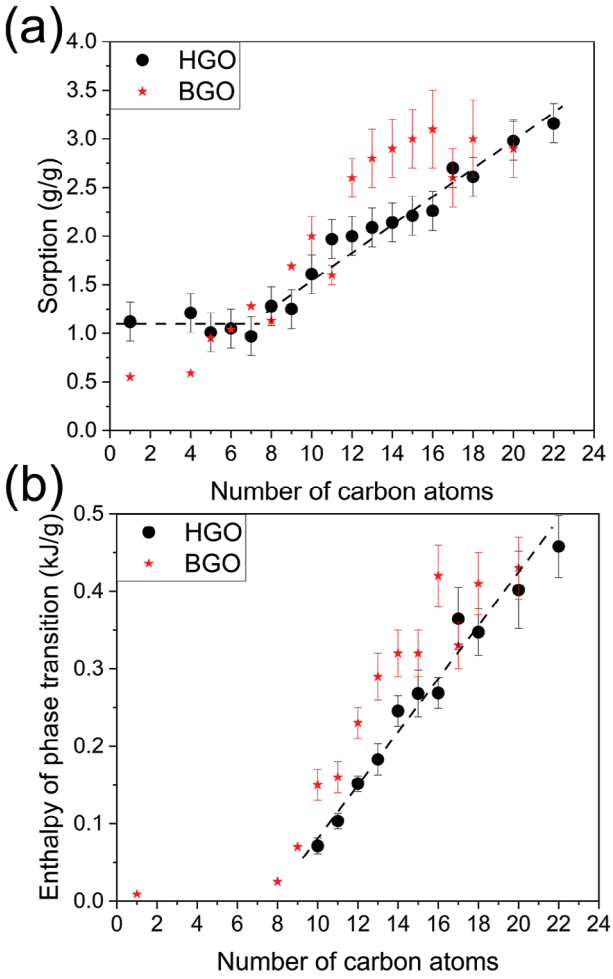

Figure 6. (a) Sorption of 1-alcohols (named according to number of carbon atoms in the chain C1–C22) by HGO (black symbols) and BGO (red symbols) near the temperature point of solvent melting. (b) Enthalpy of swelling transitions evaluated using DSC for HGO and BGO in liquid 1-alcohols. HGO shows no phase transitions for alcohols C1–C9.

HGO systems with smaller (<10) alcohols should be explained by intrinsically inhomogeneous distribution of oxygen-containing functional groups over the graphene skeleton. The presence of non-oxidized graphene regions in HGO prevents formation of well-defined solvent layers of small alcohols. In contrast, BGO is known to be oxidized more homogeneously[9b] and demonstrates swelling transitions in several alcohols.

The shortest alcohols (methanol, ethanol, and propanol) are hydrophilic and water-miscible thus forming a group of its own in relation to swelling of BGO and HGO. Effects of random interstratification and "intrastratification" (inhomogeneous hydration within one inter-layer)[28b] are especially strong for HGO swelling in smallest alcohols emphasizing inhomogeneous nature of this material. The HGO can be imagined as a mixture of differently oxidized materials on nm-scale where each microscopic part represents "material" with different temperature point of swelling transition. The continuous shift of d(001) is then a result of averaging over many microscopic parts of the sample experiencing swelling transitions at different temperature points. This model is in agreement with all experimental observations but requires further more direct confirmations.

3. Conclusion

Temperature-dependent Swelling of HGO in a set of 1-alcohols starting from C1 (methanol) and up to C22 (behenyl alcohols) was studied using in situ synchrotron radiation XRD and DSC. The main results are summarized as follows:

1) HGO swells in all liquid alcohols in the C1–C22 set with progressively larger expansion of c-lattice. The maximal interlayer distance of 63.6 Å was found for HGO-C22. Larger expansion of c-lattice correlates with stronger sorption of alcohols determined using by the DSC method.
2) The structure of low-temperature α-phases is preserved after solidification of alcohols C4–C22, thus providing solid solvate phases of HGO intercalated with alcohol molecules at ambient temperatures.
3) Swelling transitions are found for HGO in longer-chain liquid alcohols (C10–C22). Remarkably, it is the first-ever example of swelling transitions reported for HGO in any polar solvents.
4) The swelling transitions are of Type II, similarly to transitions reported previously for BGO. The reversible transitions from low-temperature α-phases into high-temperature β-phases occur with significant decrease of d(001), change in orientation of alcohol molecules from perpendicular to parallel to GO layers, and partial removal of alcohol from the HGO inter-layers.
5) The swelling transitions observed during the heating correspond to incongruent melting of α-phase and loss of partial ordering of intercalated solvent molecules.
6) In contrast to BGO, no swelling transitions are found for HGO in smaller alcohols C1–C9.
7) The d(001) of HGO intercalated with smallest alcohols (C1–C3) shows significant but continuous changes during the cooling and heating. The temperature dependence of d(001)

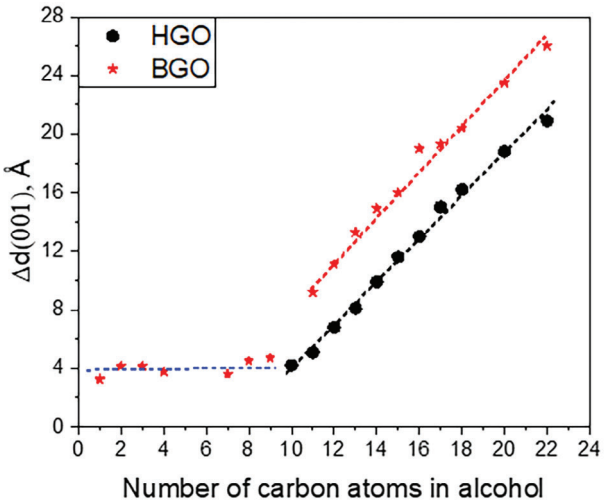

Figure 7. Changes of interlayer distance Δd(001) at the point of swelling transitions for HGO (black symbols) and BGO (red symbols) plotted as a function of 1-alcohol molecules length provided by the number of carbon atoms in the chain (C1–C22).

for HGO in C4–C9 alcohols shows smaller changes. The gradual changes of d(001) with increments much smaller than the size of solvent molecules are explained in a terms of interstratification.

Our study provides the most comprehensive overview of swelling for HGO in a set of 1-alcohols and discusses similarities and differences compared to swelling of BGO in the same alcohols. The main difference is found for swelling in smaller alcohols, presumably due to more homogeneous oxidation of BGO and uneven distribution of oxidized areas and non-oxidized islands on the surface of HGO flakes. We note that this study is limited to HGO phases formed in excess of liquid alcohols due to saturated swelling, while variety of solvent-deficient phases can possibly be found in each alcohol similarly to earlier studied BGO-C16 system.[23b]

HGO is mostly used in experimental studies related to applications of graphene oxide. Therefore, our results are of fundamental value also for variety of membrane applications based on using multilayered graphene oxide foils. We demonstrate that inter-layer distance of HGO can be increased by swelling in alcohols producing a wide range of values at least up to ≈64 Å and tuned with high precision by selection of intercalating alcohol molecules. However, swelling of HGO multilayered films and membranes is not necessarily the same as in precursor graphite oxides and needs to be verified experimentally.

4. Experimental Section

The HGO batch used in this study was purchased from Abalonyx and characterized using XRD, XPS, TGA/DSC (Figures S1–S3, Supporting Information). Shortly, all characterization methods confirmed rather standard for Hummer's GO properties of precursor material with overall C/O = 1.99 with some sulfur impurity (0.94 at%). Excluding oxygen from sulfate groups gives C/O = 2.24.

XPS spectra were recorded with a Kratos Axis Ultra electron spectrometer equipped with a delay line detector. A monochromatic Al Kα source operated at 150 W, a hybrid lens system with a magnetic lens, providing an analysis area of 0.3 × 0.7 mm, and a charge neutralizer was used for the measurements. The binding energy scale was adjusted with respect to the C1s line of aliphatic carbon, set at 285.0 eV. All spectra were processed with the Kratos software. TGA was done using a Mettler Toledo TGA/DSC1 STARe System. Experiments were performed from room temperature up to 900 °C at a heating rate of 5 K min^{-1} under nitrogen flow (20 mL min^{-1}).

DSC scans of HGO in various alcohols (from C1 to C22) were recorded using a STARe system DSC 3 by Mettler Toledo under flow of nitrogen with heating/cooling rate 2 K min^{-1}. Samples were typically studied for three cycles and the values for enthalpies and temperature reported in the manuscript were from the third heating/cooling cycle. The BGO/alcohol mixtures were studied using aluminum DSC capsules. The uncertainty for sorption values and enthalpy of transition was calculated assuming that the main errors were due to balance accuracy (0.1 mg) and assuming 95% confidence interval.

Experiments with HGO in C17 and C20 were performed at the Rossendorf Beamline (BM20),[34] ESRF, using a Cryostream 800 System (Oxford Cryosystems) and an X-ray wavelength of λ = 0.7381 Å (16.798 keV). Experimental data with heating and cooling (rate: 1 K min^{-1}, exposure time: 10 s) were collected in transmission geometry using a DECTRIS PILATUS3 × 2 M Si area detector and extracted with the Bubble software. The detector geometry parameters were calibrated with PyFAI using the NIST LaB6 standard reference material. The intensity of the X-ray beam was adjusted using filters to avoid beam-induced damage.

Experiments with HGO in C1–C13 were collected at beamline ID22 at the European Synchrotron Radiation Facility[35] using a Perkin Elmer XRD 1611CP3 detector positioned at a distance of 1400 mm from the sample. The X-ray wavelength was calibrated as 0.354352(4) Å (35 keV) via a NIST standard 640c Si powder. Diffraction patterns were collected during time-resolved experiments with typical parameters as follows: five frames by 2 s (0.4 s per frame) and 120 s waiting time, thus providing one XRD image in about every 2 min. Azimuthal integration was carried out using the PyFAI library. The heating and cooling rate was 1 K min^{-1}.

The rest of the data were recorded at the DanMAX beamline at the MAX IV Laboratory. The temperature with heating and cooling rate 1 K min^{-1} was controlled using a Cryostream 800+ (Oxford Cryosystems). The diffraction data (10 frames per 1 s) were collected up to a maximum 2θ of 28° (Q_{max} ≈3.75 Å^{-1}) using a wavelength of 0.8266 Å (15 keV) on a DECTRIS PILATUS3 × 2 M CdTe area detector. The wavelength and geometry of the instrument were refined using a LaB_6 standard (NIST SRM660c) using the program PyFAI. The raw area detector data were azimuthally integrated to intensity versus 2θ using the MatFRAIA algorithm. The beam was attenuated to avoid radiation-induced damage to the samples.

Glass capillaries with diameters of 0.7–1 mm and transmission geometry were used in all of XRD experiments at ESRF and at MAX IV. Typically, the powder samples of HGO and solid alcohols were ground together in proportion providing excess of solvent for saturated swelling, loaded into glass capillaries which were sealed to prevent solvent evaporation at higher temperatures. The mixture was then heated above the melting point of alcohol using a controlled temperature ramp with simultaneous recording of XRD images. In the case if alcohol was liquid at room temperature, the procedure was similar, except that liquid solvent was added to the powder directly inside of capillary.

Supporting Information

Supporting Information is available from the Wiley Online Library or from the author.

Acknowledgements

A.T. acknowledges the Vibrational Spectroscopy Platform of Umeå University and A. Shchukarev for support with the XPS characterization. The authors acknowledge MAX IV Laboratory for time on Beamline DanMAX under Proposal 20210963 and ESRF for time at BM20 (ROBL) beamline, ID22 beamline (proposal HC-5403). The authors thank Mads Ry Vogel Jørgensen and Innokenty Kantor for support of experiments at MAX IV. European Union's Horizon 2020 research and innovation program under grant agreement no. 881603 (ATN), Energimyndigheten grant (No. 50620–1) (ATN). Research conducted at MAX IV was supported by the Swedish Research Council under contract 2018–07152, the Swedish Governmental Agency for Innovation Systems under contract 2018–04969, and Formas under contract 2019–02496. DanMAX is funded by the NUFI grant no. 4059-00009B.

Conflict of Interest

The authors declare no conflict of interest.

Author Contributions

A.I. and A.N. contributed equally to this work. A.V.T. conceptualized the study. A.V.T. and C.H. developed the methodology. A.I., A.N., N.B., G.L., and A.V.T. conducted the investigation. A.I., A.N., G.L., and A.V.T. handled the visualization. A.V.T. supervised the project. A.V.T. and G.L. wrote the original draft. All authors reviewed and edited the manuscript.

Data Availability Statement

The data that support the findings of this study are available in the supplementary material of this article.

Keywords

alcohols, graphene, graphene oxide, swelling, X-ray diffraction

Received: August 6, 2024
Revised: September 16, 2024
Published online: September 24, 2024

[1] B. C. Brodie, *Philos. Trans. R. Soc. London* **1859**, *149*, 249.
[2] W. S. Hummers, R. E. Offeman, *J. Am. Chem. Soc.* **1958**, *80*, 1339.
[3] B. Gurzeda, N. Boulanger, M. R. V. Jorgensen, I. Kantor, A. V. Talyzin, *Carbon* **2024**, *221*, 118899.
[4] B. Gurzeda, P. Florczak, M. Kempinski, B. Peplinska, P. Krawczyk, S. Jurga, *Carbon* **2016**, *100*, 540.
[5] S. J. You, S. M. Luzan, T. Szabo, A. V. Talyzin, *Carbon* **2013**, *52*, 171.
[6] H. P. Boehm, W. Scholz, *Z. Anorg. Allg. Chem.* **1965**, *335*, 74.
[7] P. Feicht, R. Siegel, H. Thurn, J. W. Neubauer, M. Seuss, T. Szabo, A. V. Talyzin, C. E. Halbig, S. Eigler, D. A. Kunz, A. Fery, G. Papastavrou, J. Senker, J. Breu, *Carbon* **2017**, *114*, 700.
[8] H. Lin, A. Iakunkov, N. Severin, A. V. Talyzin, J. P. Rabe, *J. Phys. Chem. C* **2022**, *126*, 20658.
[9] a) A. V. Talyzin, T. Hausmaninger, S. J. You, T. Szabo, *Nanoscale* **2014**, *6*, 272; b) A. V. Talyzin, G. Mercier, A. Klechikov, M. Hedenstrom, D. Johnels, D. Wei, D. Cotton, A. Opitz, E. Moons, *Carbon* **2017**, *115*, 430; c) A. V. Talyzin, A. Klechikov, M. Korobov, A. T. Rebrikova, N. V. Avramenko, M. F. Gholami, N. Severin, J. P. Rabe, *Nanoscale* **2015**, *7*, 12625; d) S. J. You, S. Luzan, J. C. Yu, B. Sundqvist, A. V. Talyzin, *J. Phys. Chem. Lett.* **2012**, *3*, 812.
[10] a) H. Y. He, J. Klinowski, M. Forster, A. Lerf, *Chem. Phys. Lett.* **1998**, *287*, 53; b) A. Lerf, H. Y. He, M. Forster, J. Klinowski, *J. Phys. Chem. B* **1998**, *102*, 4477; c) T. Szabo, O. Berkesi, P. Forgo, K. Josepovits, Y. Sanakis, D. Petridis, I. Dekany, *Chem. Mater.* **2006**, *18*, 2740.
[11] a) A. Klechikov, J. C. Yu, D. Thomas, T. Sharifi, A. V. Talyzin, *Nanoscale* **2015**, *7*, 15374; b) A. Iakunkov, A. V. Talyzin, *Nanoscale* **2020**, *12*, 21060.
[12] J. C. Ruiz, D. M. C. Macewan, *Nature* **1955**, *176*, 1222.
[13] U. Hofmann, A. Frenzel, E. Csalán, *Justus Liebigs Ann. Chem.* **1934**, *510*, 1.
[14] a) H. P. Boehm, A. Clauss, U. Hofmann, *J. Chim. Phys.* **1961**, *58*, 141; b) R. K. Joshi, P. Carbone, F. C. Wang, V. G. Kravets, Y. Su, I. V. Grigorieva, H. A. Wu, A. K. Geim, R. R. Nair, *Science* **2014**, *343*, 752; c) Z. T. Luo, Y. Lu, L. A. Somers, A. T. C. Johnson, *J. Am. Chem. Soc.* **2009**, *131*, 898; d) H. W. Kim, H. W. Yoon, S. M. Yoon, B. M. Yoo, B. K. Ahn, Y. H. Cho, H. J. Shin, H. Yang, U. Paik, S. Kwon, J. Y. Choi, H. B. Park, *Science* **2013**, *342*, 91; e) H. Li, Z. N. Song, X. J. Zhang, Y. Huang, S. G. Li, Y. T. Mao, H. J. Ploehn, Y. Bao, M. Yu, *Science* **2013**, *342*, 95; f) Y. P. Tang, D. R. Paul, T. S. Chung, *J. Membrane Sci.* **2014**, *458*, 199.
[15] a) A. Iakunkov, J. H. Sun, A. Rebrikova, M. Korobov, A. Klechikov, A. Vorobiev, N. Boulanger, A. V. Talyzin, *J. Mater. Chem. A* **2019**, *7*, 11331; b) H. Lin, A. Iakunkov, N. Severin, A. V. Talyzin, J. P. Rabe, *J. Phys. Chem. C* **2022**, *126*, 20658.
[16] A. A. Eliseev, A. A. Poyarkov, E. A. Chernova, A. A. Eliseev, A. P. Chumakov, O. V. Konovalov, D. I. Petukhov, *2d Mater* **2019**, *6*, 035039.
[17] E. A. Chernova, D. I. Petukhov, A. P. Chumakov, A. V. Kirianova, I. S. Sadilov, O. O. Kapitanova, O. V. Boytsova, R. G. Valeev, S. V. Roth, A. A. Eliseev, A. A. Eliseev, *Carbon* **2021**, *183*, 404.
[18] a) C. A. Amadei, C. D. Vecitis, *J. Phys. Chem. Lett.* **2016**, *7*, 3791; b) A. V. Kaplin, A. T. Rebrikova, E. A. Eremina, N. A. Chumakova, N. V. Avramenko, M. V. Korobov, *Membranes (Basel)* **2023**, *13*, 53.
[19] a) A. V. Talyzin, V. L. Solozhenko, O. O. Kurakevych, T. Szabo, I. Dekany, A. Kurnosov, V. Dmitriev, *Angew. Chem. Int. Ed.* **2008**, *47*, 8268; b) A. V. Talyzin, B. Sundqvist, T. Szabo, I. Dekany, V. Dmitriev, *J. Am. Chem. Soc.* **2009**, *131*, 18445; c) A. V. Talyzin, B. Sundqvist, T. Szabo, V. Dmitriev, *J. Phys. Chem. Lett.* **2011**, *2*, 309.
[20] J. Zhu, C. M. Andres, J. D. Xu, A. Ramamoorthy, T. Tsotsis, N. A. Kotov, *ACS Nano* **2012**, *6*, 8357.
[21] a) A. Vorobiev, A. Dennison, D. Chernyshov, V. Skrypnychuk, D. Barbero, A. V. Talyzin, *Nanoscale* **2014**, *6*, 12151; b) M. V. Korobov, A. V. Talyzin, A. T. Rebrikova, E. A. Shilayeva, N. V. Avramenko, A. N. Gagarin, N. B. Ferapontov, *Carbon* **2016**, *102*, 297; c) S. J. You, B. Sundqvist, A. V. Talyzin, *ACS Nano* **2013**, *7*, 1395; d) A. V. Talyzin, S. M. Luzan, *J. Phys. Chem. C* **2010**, *114*, 7004; e) C. Cabrillo, F. Barroso-Bujans, R. Fernandez-Perea, F. Fernandez-Alonso, D. Bowron, F. J. Bermejo, *Carbon* **2016**, *100*, 546.
[22] a) S. J. You, J. C. Yu, B. Sundqvist, L. A. Belyaeva, N. V. Avramenko, M. V. Korobov, A. V. Talyzin, *J. Phys. Chem. C* **2013**, *117*, 1963; b) A. T. Rebrikova, A. Klechikov, A. Iakunkov, J. H. Sun, A. V. Talyzin, N. V. Avramenko, M. Korobov, *J. Phys. Chem. C* **2020**, *124*, 23410; c) A. Klechikov, J. H. Sun, I. A. Baburin, G. Seifert, A. T. Rebrikova, N. V. Avramenko, M. V. Korobov, A. V. Talyzin, *Nanoscale* **2017**, *9*, 6929; d) F. Aragon, J. C. Ruiz, D. M. C. Macewan, *Nature* **1959**, *183*, 740.
[23] a) A. Iakunkov, A. Nordenström, N. Boulanger, G. Li, C. Hennig, M. R. V. Jorgensen, I. Kantor, A. V. Talyzin, *Adv. Mater. Interfaces* **2024**, *11*, 2300554; b) A. Nordenstrom, A. Iakunkov, N. Boulanger, G. Li, C. Hennig, I. Baburin, M. Jorgensen, I. Kantor, A. V. Talyzin, *Carbon* **2023**, *203*, 770; c) A. Iakunkov, A. Nordenström, N. Boulanger, G. Li, C. Hennig, M. R. V. Jorgensen, I. Kantor, A. V. Talyzin, *Adv. Mater. Interfaces* **2023**, *11*, 2300554.
[24] L. Staudenmaier, *Ber. Dtsch. Chem. Ges* **1898**, *31*, 1481.
[25] R. Kruger, PhD thesis at Ludwig-Maximilians-Universität München **1980**.
[26] A. R. Garcia, J. Canoruiz, D. M. C. Macewan, *Nature* **1964**, *203*, 1063.
[27] A. Lerf, A. Buchsteiner, J. Pieper, S. Schöttl, I. Dekany, T. Szabo, H. P. Boehm, *J. Phys. Chem. Solids* **2006**, *67*, 1106.
[28] a) B. Rezania, N. Severin, A. V. Talyzin, J. P. Rabe, *Nano Lett.* **2014**, *14*, 3993; b) A. V. Talyzin, *Nat. Nanotechnol.* **2022**, *17*, 131.
[29] A. Lerf, A. Buchsteiner, J. Pieper, S. Schottl, I. Dekany, T. Szabo, H. P. Boehm, *J. Phys. Chem. Solids* **2006**, *67*, 1106.
[30] a) J. L. Mcatee, *Am. Mineral.* **1956**, *41*, 627; b) G. Brown, D. M. C. Macewan, *J. Soil Sci.* **1950**, *1*, 239.
[31] S. Célérier, S. Hurand, C. Garnero, S. Morisset, M. Benchakar, A. Habrioux, P. Chartier, V. Mauchamp, N. Findling, B. Lanson, E. Ferrage, *Chem. Mater.* **2019**, *31*, 454.
[32] A. V. Talyzin, S. M. Luzan, T. Szabo, D. Chernyshev, V. Dmitriev, *Carbon* **2011**, *49*, 1894.
[33] K. Erickson, R. Erni, Z. Lee, N. Alem, W. Gannett, A. Zettl, *Adv. Mater.* **2010**, *22*, 4467.
[34] A. C. Scheinost, J. Claussner, J. Exner, M. Feig, S. Findeisen, C. Hennig, K. O. Kvashnina, D. Naudet, D. Prieur, A. Rossberg, M. Schmidt, C. Qiu, P. Colomp, C. Cohen, E. Dettona, V. Dyadkin, T. Stumpf, *J. Synchrotron Radiat.* **2021**, *28*, 333.
[35] A. Fitch, C. Dejoie, E. Covacci, G. Confalonieri, O. Grendal, L. Claustre, P. Guillou, J. Kieffer, W. de Nolf, S. Petitdemange, M. Ruat, Y. Watier, *J. Synchrotron Radiat.* **2023**, *30*, 1003.